*J. Fluid Mech.* (1970), *vol.* 44, *part* 1, *pp.* 129–144
*Printed in Great Britain*



# Pressure measurements in the water-entry cavity

By H. I. ABELSON†

U.S. Naval Ordnance Laboratory
White Oak, Silver Spring, Maryland

(Received 22 January 1970)

Significant experimental results from a study of pressure in the water-entry cavity are presented. Projectiles were fired into water at velocities up to 250 ft./sec and entry angles of 90°, 60°, and 45°. Pressure data obtained using underwater probes were correlated with high-speed motion pictures taken of the entries. Results indicate that the cavity pressure drop prior to surface closure is an order of magnitude greater than previously assumed. As the entry angle is decreased from 90°, the pressure drop decreases. The minimum cavity pressure decreases linearly with increasing entry velocity over the test range. As the entry angle is increased, the minimum entry velocity required to produce a measurable pressure drop becomes greater. An improved pressure-volume correlation is obtained if the volume enclosed by the cavity walls is corrected to account for re-entrant jet volume and air volume enclosed by the splash walls. Cavity pressure during the closed cavity phase behaves approximately according to the isentropic pressure–volume relation. Pressure drop and history are strongly dependent on projectile nose geometry. No appreciable cavity pressure gradient, axial or transverse, was found to exist. Deep closure or cavity collapse is accompanied by relatively high-pressure pulses.

## Introduction

Literature relating to the water-entry cavity contains mostly brief qualitative statements concerning the pressure in the cavity. Birkhoff & Isaacs (1951) and Abelson (1969) attempt to estimate this pressure; Richardson (1948) and Hoover & Dawson (1966) report only two isolated measurements. Birkhoff (1946), May (1952) and Abelson (1969) discuss water-entry cavity behaviour in detail.

A frequently stated assumption is that the cavity pressure drop prior to surface closure is very small and approximately equal to $\frac{1}{2}\rho_a u_0^2$ where $\rho_a$ is the normal air density and $u_0$, the projectile entry velocity. After surface closure, when the cavity is sealed off from the atmosphere, it has been assumed that the pressure behaves according to the isentropic relation $p_c V_c^\gamma = \text{const}$. Here the cavity pressure $p_c$ is assumed to be constant throughout the cavity at any given instant of time. Nothing regarding pressure gradients in the open cavity phase is discussed in the literature.

Richardson (1948) attempted to measure cavity pressure by dropping an

† Present address: Department of Mechanical Engineering, Manhattan College, Riverdale, New York.

instrumented projectile into water. Data were reported for a single entry at 20 ft./sec and showed that the pressure remained nearly atmospheric until deep closure occurred, at which time damped pressure oscillations began. For this special case, a very low velocity entry, neither surface closure nor pullaway occurs. Hoover & Dawson (1966) made some preliminary pressure measurements in cavities formed by dropping spheres into water, and found that the cavity pressure did deviate from the atmospheric value while the cavity was open.

The performance of water-entry projectiles is affected by the cavities which form behind them. The control of cavity behaviour may be accomplished through some modification of cavity pressure. Cavity closures and collapse, with attendant acoustic phenomena, can only be understood when pressure values are known. In this paper, a presentation of significant experimental results obtained from an extensive study of cavity pressure at vertical and oblique entry will be made.

## Experimental programme

Tests were conducted in which a 3 in. diameter, 140° conical-nosed projectile was fired into water at velocities up to 250 ft./sec and at entry angles of 90°, 60°, and 45° from the water surface. Several entries were also made using a hemispherical-nosed projectile of similar size to determine the effect of nose shape on cavity pressure. Two methods of pressure measurement were employed. The first involved placing probes (housing piezo-electric pressure transducers) under water at such locations as to become enveloped in the expanding cavity, a technique used by Hoover & Dawson (1966). The flexibility of the system allowed probes to be positioned so as to penetrate the cavity wall at chosen depths, times, and distances from the line of fire. The use of several probes simultaneously permitted the study of cavity pressure gradients. Tests showed that the presence of probes had no visible effect on cavity behaviour, provided the probe-to-projectile-diameter ratio was kept small. In order to correlate pressure data with cavity behaviour, high-speed motion pictures were taken of each entry with a clock placed in the field of view. The camera lens was positioned to split the water surface, permitting the observation of splash behaviour as well as events below the water surface. A schematic of the probe method for vertical entry is shown in figure 1.

The second method of pressure measurement employed an instrumented projectile with a piezo-electric transducer flush-mounted in its side. The projectile had the same weight and geometry as that used in the probe method, and signals were carried to the recording devices by means of trailing cable. Though the instrumented-model method offers the advantage of providing a continuous pressure record from water impact on, it does not lend itself to the study of cavity pressure gradients. Numerous difficulties were encountered, with meaningful pressure data being obtained for only a few entries. Difficulties included cable breakage at moderate entry velocities, cable whip preventing or delaying surface closure, and base line shifting due to transducer temperature sensitivity. The results to be presented here will be based, therefore, on data obtained using the

probe method. Instrumented-model data for a single entry will be compared with probe data for a corresponding entry, however, in order to provide a check on the latter. The particular nose shape used, the 140° cone, was chosen because of its stability after water entry and the relatively wide cavity it generates. A wide cavity allows for more strategic positioning of probes, while a stable projectile offers no threat of probe damage. Tank dimensions limited the range of entry velocities because wall effects, occurring with the large cavities generated at high speeds, prevented normal cavity expansion. Depth limitations permitted

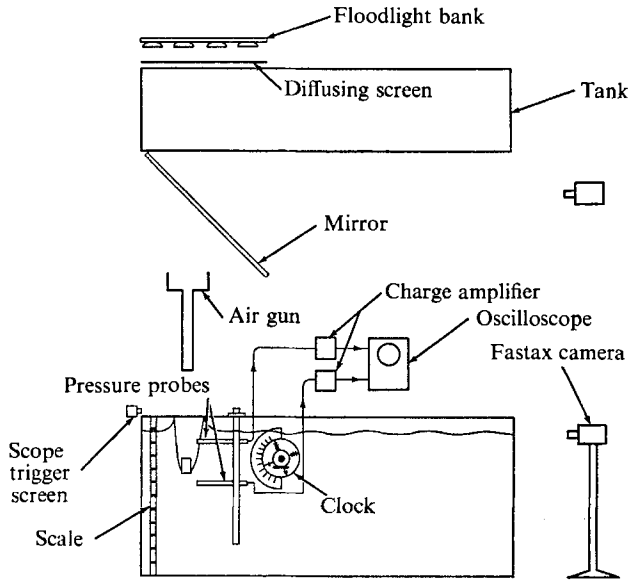


FIGURE 1. Apparatus schematic for probe method of cavity pressure measurement.

cavity behaviour to be studied only prior to deep closure. Restrictions on the velocity range were also imposed because of base line shifting in signals from probes placed at shallow depths, due to the severe water-impact shock produced at high velocities. Preliminary tests, using a flat-nosed cylindrical projectile, indicated that base line shifting occurred even at relatively low-entry velocities and moderate probe depths, because of the high-impact shock associated with the flat nose.

## Experimental results

### *Typical pressure data*

Figure 2 (plate 1) shows typical pressure data obtained from a vertical entry at 145 ft./sec. The upper and lower traces correspond to signals from probes placed at 3 in. and 15 in. depths, respectively. Repeatability of pressure data and observed cavity behaviour (on film) was excellent over the entire range of entry velocities. In figure 3, cavities sketched from motion pictures taken of the above entry, showing the relative positions of the probes, are correlated with the pressure data of figure 2. Point 1 corresponds to water impact. It is noted that the rapid rise and fall in pressure observed in both probe signals just after impact

does not correspond to cavity pressure, since the probes have not yet penetrated the cavity wall. The minimum cavity pressure, point 5, occurs shortly after the estimated time of surface closure. Only a rough estimate of the time of surface closure can be obtained from motion pictures of the entry, because of the opaqueness of the splash walls and the presence of residual spray (see figure 5, plate 2). The jet observed travelling down the centre of the cavity in frames 4 and 5 of figure 3 is, in reality, a spray of water droplets from the splash that have become entrained in the airflow. A true re-entrant jet is formed after pullaway in frame 6. Only residual spray remains above the water surface after this time. A rise in pressure above the local hydrostatic (base line) value is observed after point 8

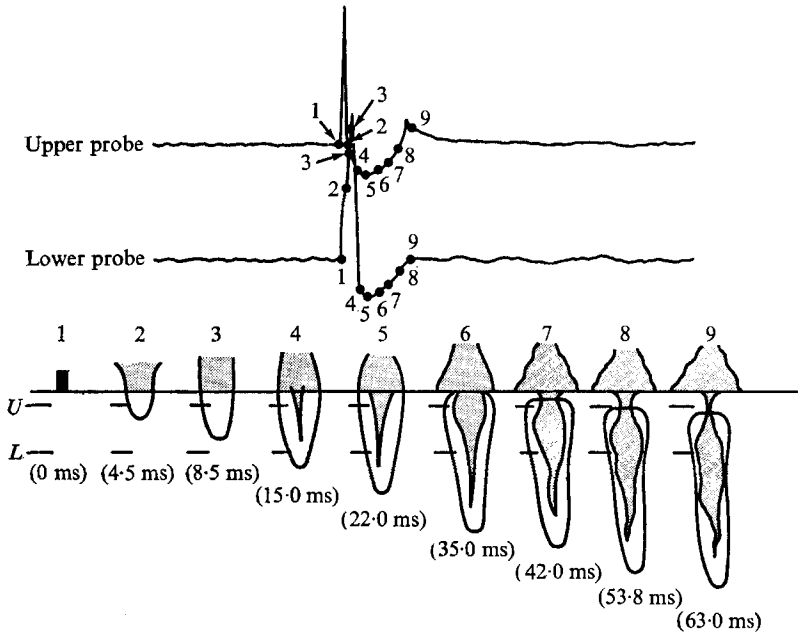


FIGURE 3. Correlation of pressure data from figure 2 with photographically observed cavity behaviour.

on the upper probe signal. The corresponding cavity sketches show that the upper probe is no longer penetrating the cavity, but, rather, is measuring pressure in the region just behind it. In ideal flow about a cavity-shaped body, this would correspond to a high-pressure region, as the measurements indicate. As the top of the cavity moves further away from the probes, the pressure returns to the local hydrostatic value. As expected, for higher entry velocities, this overshoot increases.

*Pressure-volume correlation*

Figure 4 shows a comparison of cavity volume and cavity pressure for the entry discussed above. The pressure signals of figure 2 have been superimposed on each other (taking into account the difference in hydrostatic pressure) and are shown in part. Cavity photographs, corresponding to the times denoted in capital letters, are shown in figure 5 (plate 2). The corresponding instantaneous

projectile velocities are noted in figure 4. Both the outline volume and true cavity volume, estimated from entry films, have been plotted here. The former equals the total volume enclosed by the cavity walls and is the quantity referred to as 'cavity volume' in the literature. For a meaningful pressure-volume correlation, only the total volume of gas (air and water vapour) in the cavity should be

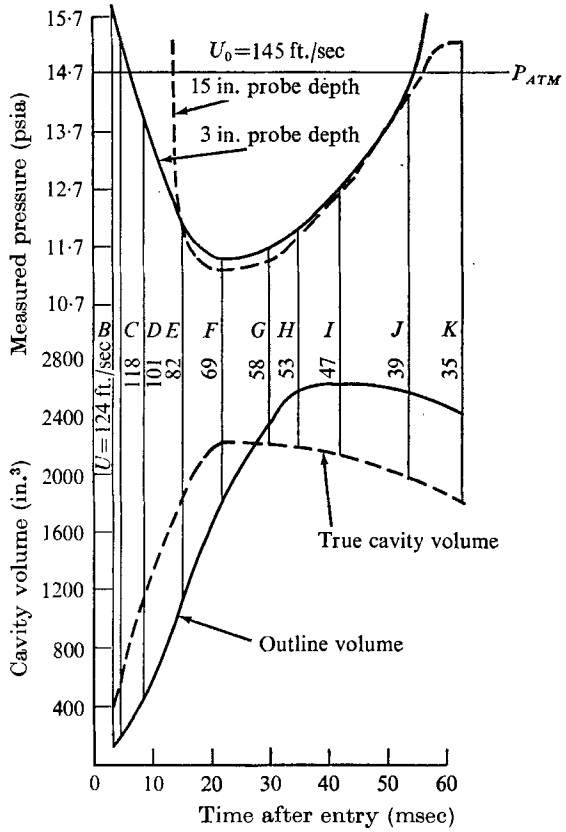


FIGURE 4. Cavity pressure-cavity volume correlation.

considered. Since the re-entrant jet is composed of liquid, its volume should not be included. At surface closure, the splash walls form a dome above the water surface, which moves downward until, at pullaway, it becomes completely submerged. Certainly, the air contained in this dome comprises part of the closed-cavity gas volume and should be estimated and included. In the open-cavity phase, the uppermost point of the splash walls, rather than the opening at the water surface, more correctly defines the flow aperture area. Thus, the air volume enclosed by the open splash walls should likewise be included. The true cavity volume is then equal to the sum of the air volume enclosed by both the cavity and splash walls, minus the re-entrant jet volume. As is evident from figure 4, a much improved pressure-volume correlation is obtained using true cavity volume. In the pressure-outline volume comparison, maximum volume and minimum pressure do not correspond in time, and it is observed that both pressure and

volume are increasing over some time interval, necessitating heat transfer to the cavity. Order-of-magnitude calculations have indicated that, for the short time durations involved, heat transfer into the cavity is negligible, even if large-cavity temperature drops are assumed.

### *Vertical vs. oblique*

In figure 6, pressure data (shown in part) from oblique entries at 60° and 45° (at 145 ft./sec) are compared with the vertical-entry data of figure 2. The circle on each curve denotes the time at which the probe appeared to penetrate the cavity wall. It is observed that, prior to probe penetration, the pressure signals are shifted more to the right as the entry angle is decreased, due to the increased distance the projectile must travel to reach a given probe depth. Consequently, the decrease in peak pressure at smaller entry angles is a result of greater projectile slowdown. Comparison of upper and lower probe pressure signals for the 60° and vertical entries shows almost identical cavity pressure, except for a short interval after probe penetration. Since pullaway occurs later at smaller entry angles, and the projectile velocity at a given depth is smaller, the sharp rise in pressure observed for the vertical entry after pullaway is not present in the oblique entry signals. Considering now the 45° entry, it is observed that the cavity pressure drop is considerably less than in the vertical and 60° cases. The pressure is also observed to return to the local hydrostatic value with less overshoot. The variation of cavity pressure drop with entry angle may be explained by considering the two factors which govern cavity pressure, namely, rate of cavity expansion and time of surface closure. Comparisons of oblique and vertical entry cavities at various times (for given projectiles and entry velocities) show that cavity shapes are almost identical prior to pullaway, except for a small section adjacent to the water surface. This implies more or less equal rates of cavity expansion at different entry angles. The time of surface closure, on the other hand, has been observed to increase as the entry angle is decreased, so it is apparent that this time is the primary factor governing cavity pressure drop. This increase in the time of surface closure is explained by the fact that the aperture at the water surface, and thus the splash aperture, is elliptical rather than circular for oblique entry. As the entry angle decreases, the major axis of the ellipse varies inversely as its sine, and thus the aperture requires a longer time to close. The minor axis of the ellipse remains the same as the diameter of the circular aperture at vertical entry. The inverse sine dependence may also explain the first slow and then rapid change in cavity pressure drop as the entry angle was decreased from 90° to 45°.

### *Pressure drop prior to surface closure*

Surface closure for the vertical entry at 145 ft./sec discussed above has been estimated to occur somewhere between 15 and 22 msec after water impact (corresponding to photographs *E* and *F* of figure 5, plate 2). Splash opaqueness and residual spray, evident in the photographs, prevent a more accurate estimate. The pressure drops corresponding to these times are 2·6 and 3·2 psi,

representing, respectively, 81 and 100 % of the maximum cavity pressure drop. An analysis of numerous entries of the present study showed that the pressure drop prior to surface closure was within this 80–100 % range. If the assumption (from the literature) is made here that the pressure drop prior to surface closure is approximately equal to $\frac{1}{2}\rho_a u_0^2$, a drop of 0·17 psi, 15 to 20 times smaller than that

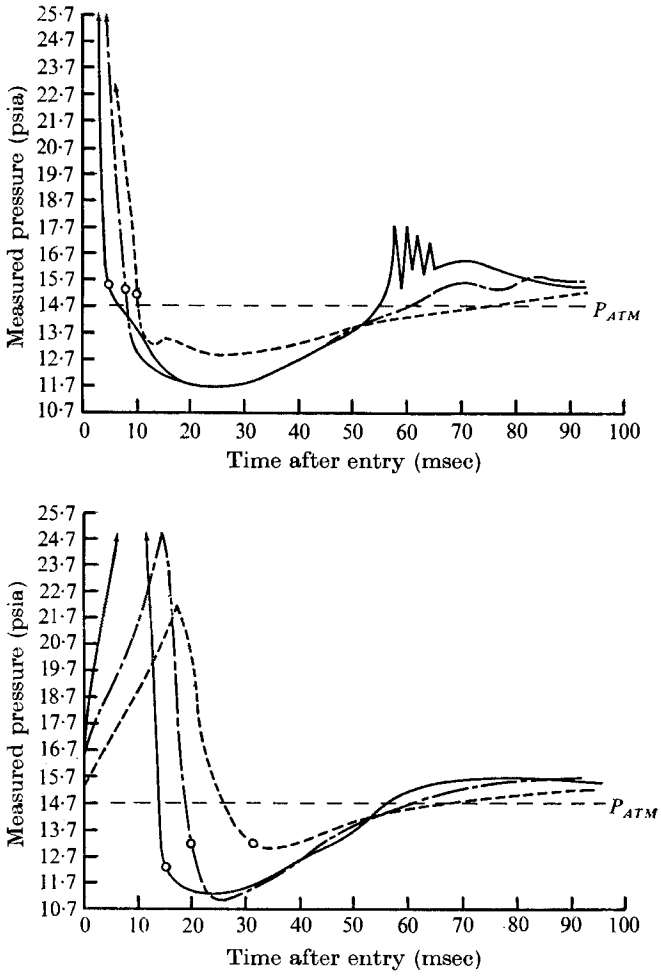


FIGURE 6. Comparison of pressure data for vertical and oblique entries. $U_0$ = 145 ft./sec. Probe depth (in.): (*a*) 3, (*b*) 15. —, vertical; — · —, oblique (60°); - - - -, oblique (45°).

measured, results. Obviously, the $\frac{1}{2}\rho_a u_0^2$ approximation is a poor one, being an order of magnitude in error. Besides not accounting for the unsteadiness of the airflow into the cavity, the $\frac{1}{2}\rho_a u_0^2$ approximation also assumes that the velocity of the airflow equals the projectile entry velocity, at most. Here the major fallacy lies, especially near surface closure, when the aperture area becomes small and the flow velocity is many times greater than the entry velocity. Nor can it be assumed beforehand that there will be a drop in cavity pressure after surface closure due to cavity expansion, unless the true cavity volume as a function of

time is known. For example, in figure 4 a decrease in cavity volume is observed shortly after surface closure, resulting in a pressure increase. It is expected that the percentage of the total pressure drop occurring prior to surface closure will be dependent on the projectile nose shape. For very low velocity entries or entries of light projectiles, where surface closure does not occur or occurs very late, the cavity pressure becomes a minimum while the cavity is open.

*Minimum cavity pressure vs. entry velocity*

Figure 7 (*a*) shows minimum cavity pressure plotted as a function of projectile entry velocity for numerous vertical entries up to 250 ft./sec. It is observed that the minimum pressure decreases almost linearly as entry velocity increases. The

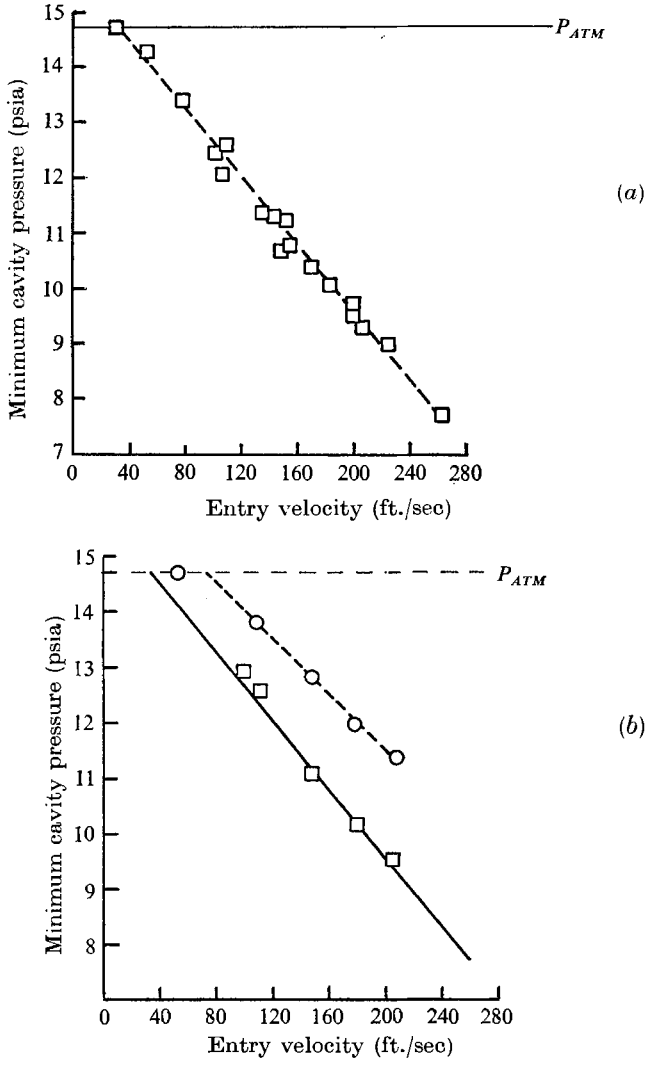


FIGURE 7. Minimum cavity pressure *vs.* entry velocity for vertical and oblique entries. —, vertical; (*a*) □, vertical. (*b*) □, 60°; ○, 45°.

best straight line through the data points has been drawn in the figure. Above velocities of 250 ft./sec, scattering of data (not shown), caused by wall effects and base line shifting due to high water-impact shock pressures, occurred. If the linear variation of minimum cavity pressure with entry velocity is extrapolated, one finds that zero pressure will occur at approximately 535 ft./sec. This could not be experimentally verified in the present test facility. Figure 7 (*b*) shows data points representing minimum cavity pressure for oblique entries at 60° and 45°. The straight line of 7 (*a*) has been drawn here to allow a comparison of vertical and oblique entry data. It is observed that the 60° data lie as close to the line as did the vertical-entry data points themselves, indicating the same linear dependence of minimum pressure on entry velocity. This is consistent with the comparisons of figure 6. For the 45° entries, the minimum cavity pressures for a given entry velocity are considerably higher than for the vertical or 60° cases, but also exhibit a linear dependence on entry speed over the range tested. Some minimum entry velocity is required before a drop in cavity pressure occurs, this value increasing as the entry angle decreases. For the vertical and 60° entries, a velocity of approximately 34 ft./sec is reached before any pressure drop occurs. If the straight line through the 45° data points is extrapolated to atmospheric pressure, the corresponding velocity of 73 ft./sec is approximately the required minimum value.

### *Cavity pressure gradients*

Figure 8 shows pressure data from a vertical entry at 151 ft./sec, in which five probes were placed at various depths to determine if an axial pressure gradient existed in the cavity. The circles denote the times the probes first penetrate the cavity wall. The probe signals have been superimposed on one another, taking into account the differences in local hydrostatic pressure. Comparing the signals from the four deepest probes, only small pressure differences are observed. The maximum difference, occurring near the minimum pressure, represents approximately 5 % of the total pressure drop. Since the signals cross over each other at several points, and do not maintain their order according to depth, the observed pressure differences are not consistent in direction and do not indicate a pressure gradient. These differences probably arise because of noise. The signal from the shallowest probe appears to deviate slightly from the others. This deviation can be attributed to a base line shift due to water-impact shock and the close proximity of the probe to the entry point. At higher entry velocities, the deviation becomes worse and cannot be interpreted as an actual pressure difference in the cavity.

To determine whether a transverse pressure gradient exists in the cavity, several entries were made where the probes were positioned at different distances from the line of fire (at the same depth). These distances were limited because of the presence of the re-entrant jet and the chance of the projectile striking the probes. Figure 9 shows pressure data for three vertical entries at 140 ft./sec where probes were placed at $2\frac{1}{4}$, 5, and $7\frac{3}{4}$ in. from the firing line, the entries being denoted by letters *A*, *B*, *C*, respectively. Motion pictures taken of entry *C* showed that both the upper and lower probes never penetrated the cavity wall. From films of entry *B* it was found that the upper probe was in the cavity during

the time interval bounded by the circled points. Over this interval, only small deviations, attributable to noise, are observed between the pressure signals of entries $B$ and $A$, indicating that no transverse gradient exists. The lower probe in entry $B$ was found to touch the cavity, although never quite penetrating it, during the interval bounded by the squared points. Agreement with the signal from entry $A$ is observed over this interval, and, again, no transverse gradient in

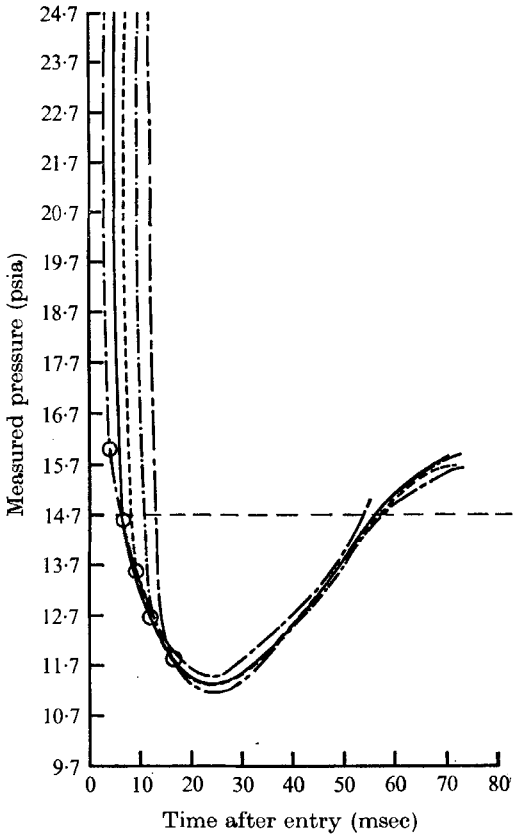


FIGURE 8. Axial pressure gradients in cavity. $U_0$ = 151 ft./sec. Probe depth (in.): — · —, 3; ——, 6; - - - -, 9; —·—, 12; — - —, 15. ○, probe enters cavity.

the cavity is indicated. The signals of entry $C$ show that, as expected, a transverse gradient does exist outside the cavity wall with the pressure increasing with distance from the line of fire until the local hydrostatic value is reached. Thus, during cavity expansion, the cavity wall moves towards a region of higher pressure and is continuously decelerated.

### *Pressure within splash*

Several entries were made with probes placed above the water surface in order to determine the pressure within the splash walls. Figure 10 shows pressure data for a vertical entry at 108 ft./sec where probes were positioned 4 in. above and 2 in. below the water surface. The upper probe becomes enveloped by the

splash almost immediately after water impact, while the lower probe penetrates the cavity wall at the time denoted by the circled point. It is observed that the pressure and splash pressure are almost identical until the minimum cavity pressure point, with the exception of a short time interval just after the probe penetrates the cavity wall. Just prior to the time minimum cavity pressure occurs,

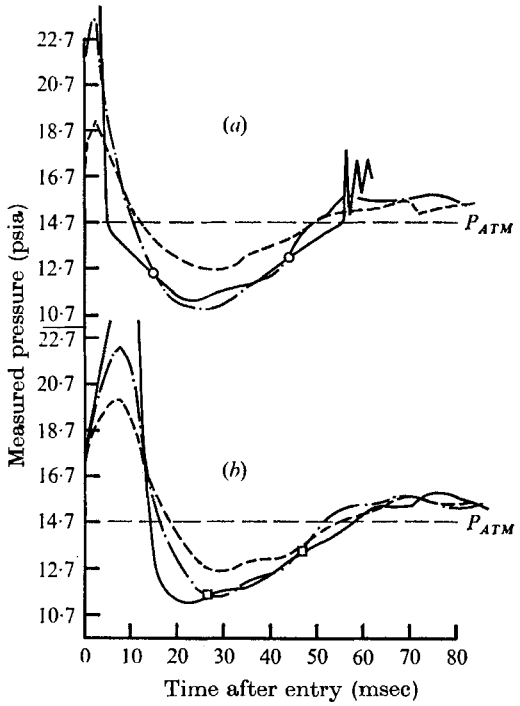


FIGURE 9. Transverse pressure gradients in cavity and surrounding flow field. $U_0$ = 140 ft./sec. Probe depth (in.): (*a*) 3, (*b*) 15. Entry: ——, *A* (2¼ in. F.L.F.); —·—, *B* (5 in. F.L.F.); - - -, *C* (7¾ F.L.F.).

a rather rapid rise in splash pressure begins, with the deviation from cavity pressure now becoming considerable. This rise in splash pressure can be explained by the fact that the dome, which forms above the water surface as a result of surface closure, moves downward until it becomes completely submerged at pullaway. In its downward motion, the dome moves away from the probe which it previously enveloped. The probe, now located amidst the residual spray, measures atmospheric pressure.

### *Closed cavity isentropic behaviour*

After surface closure, it is generally assumed that the cavity pressure behaves according to the isentropic relation $p_c V_c^{\gamma} = \text{const}$ where $\gamma = 1{\cdot}4$ for air. After deep closure, when cavity attrition begins, this relation does not apply since there is no longer a fixed mass of gas in the cavity. To determine whether the above relation is, indeed, a good approximation to closed cavity behaviour, measured cavity pressure, corresponding to the vertical entry at 145 ft./sec

discussed earlier, is compared with pressure calculated from the isentropic relation in figure 11. Here, true cavity volume, estimated from entry films, was used. The initial condition has been taken at the minimum pressure point rather than at the time of surface closure since the latter is difficult to estimate. The cavity was, of course, found to be closed at this point. In figure 11, it is seen that the calculated pressure remains lower than the measured pressure, the maximum deviation corresponding to a percentage difference of 5 %, based on the absolute pressure. The observed deviations are attributed to errors in estimation of true

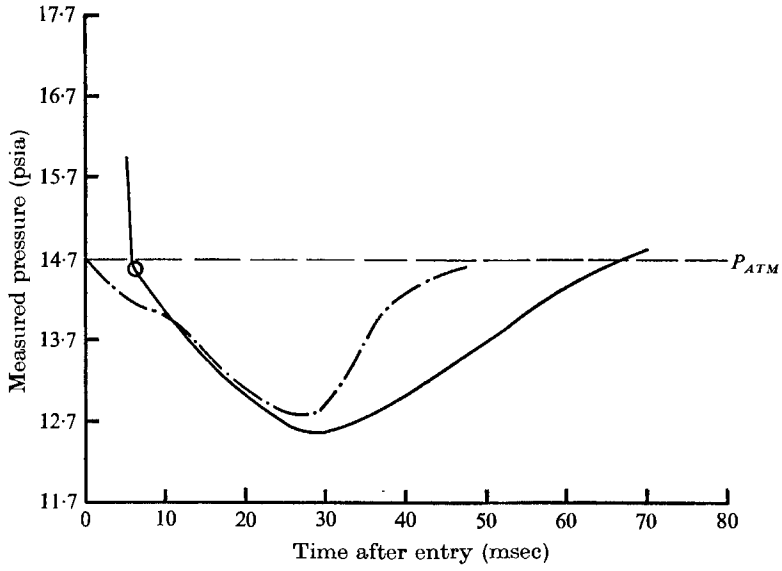


FIGURE 10. Comparison of cavity pressure and pressure within splash sheath. $U_0 = 108$ ft./sec. ——, 'cavity' probe; — · —, 'splash' probe.

cavity volume, particularly in the re-entrant jet factor. The 'fitted' volume, obtained by proceeding inversely and calculating the volume from the measured pressure, indicates the small error in volume estimation that generates the observed pressure deviations. The curves in figure 11 have been terminated at the time shown due to difficulties in estimating cavity volume because of increasing cavity wall roughness and opaqueness.

### *Effect of nose shape*

In figure 12, pressure data from the 145 ft./sec vertical entry discussed above are compared with data from an entry of a similar-sized hemispherical-nosed projectile at the same speed. It is observed that the pressure drop in the cavity is approximately 50 % greater for the hemispherical nose. Comparison of entry films shows that surface closure occurs earlier for the hemispherical-nosed projectile, but the cavity that it generates is smaller. Again, as in the vertical-oblique entry comparisons discussed earlier, the time of surface closure rather than the rate of cavity expansion is the dominant factor controlling cavity pressure drop. Why surface closure occurs earlier for the hemispherical nose may

be understood by considering two factors which govern surface closure, namely, the initial splash configuration and the aperture size at the water surface. Both factors are functions of the nose geometry. A wider cavity with a resultant larger aperture at the water surface, around which the lower end of the splash walls remain attached, will increase the time of surface closure, as will an initial splash configuration where the walls form a smaller angle with the water surface. In

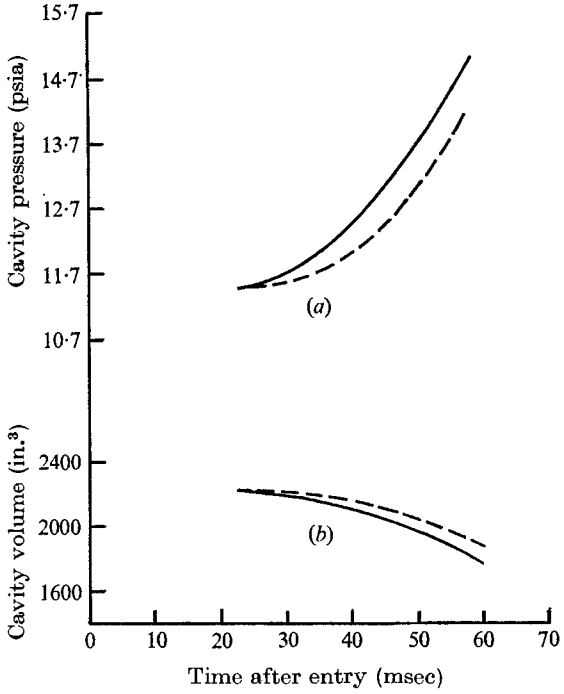


FIGURE 11. Isentropic pressure-volume behaviour during closed cavity phase ($p_c V_c^{\gamma}$ = const.). $U_0$ = 145 ft./sec.
(*a*) ——, measured; - - - -, calculated. (*b*) —, fitted; - - - -, estimated from motion pictures.

both cases, the splash walls must travel a greater distance in order to form a closure. The entry films showed that the 140° conical nose produced a large aperture, while the initial splash wall divergence appeared the same for both projectiles.

In figure 12, a sharp rise in pressure is observed in both upper and lower probe signals of the hemispherical-nose entry. The increase in the upper signal is mainly a result of the top of the cavity moving downward, away from the probe, leaving it in the high-pressure region just behind the cavity. The pressure rise at the lower probe, occurring shortly afterwards, is of greater magnitude, comparable to the pressure rise observed after entry in this case. Figure 13 (plate 3) shows the cavity and relative positions of the probes at this time. The rear of the cavity is irregular in shape and is apparently in the process of deep closure or collapse. The pressure is observed to decay rapidly from its peak, in the form of damped pressure oscillations. The above data thus indicate that high-pressure pulses are

associated with cavity collapse. The rise at the upper probe, though not initiated by the same phenomenon, has probably been sustained longer because of it. Similar pressure behaviour has not been observed for the 140° conical-nose

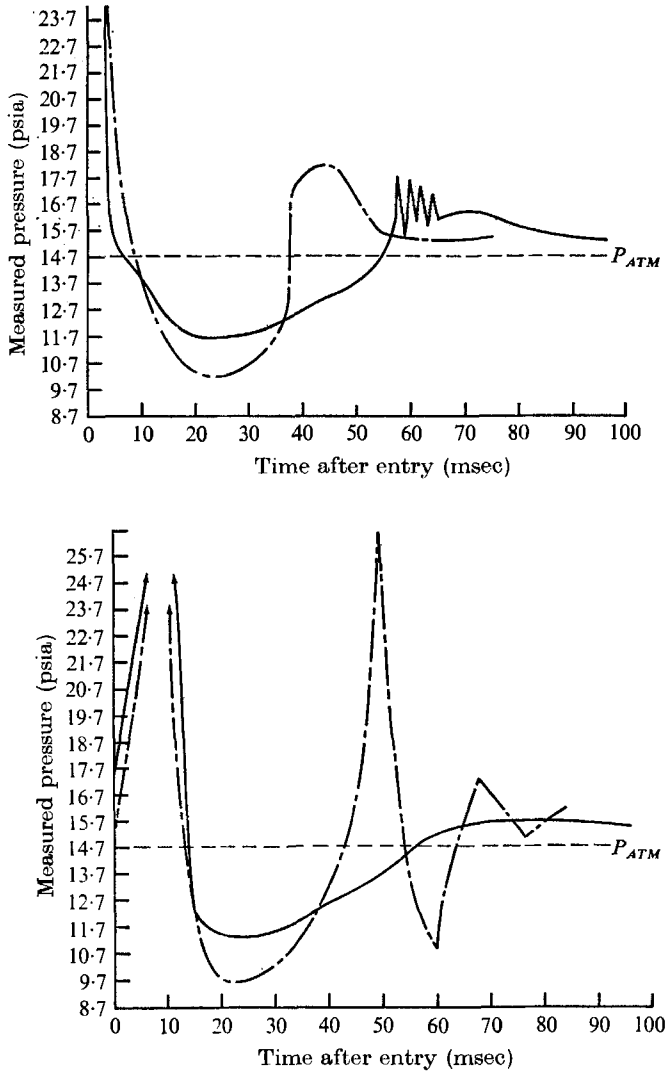


FIGURE 12. Effect of projectile nose geometry on cavity pressure. $U_0 = 145$ ft./sec. Probe depth (in.): (*a*) 3, (*b*) 15. ——, 140° conical nose; — · —, hemispherical nose.

entries, as figure 12 indicates, simply because of the depth limitation of the present test facility. Deep closure for the 140° cone occurs later than for the hemisphere, and, over the range of entry velocities tested, the projectile strikes the tank before deep closure begins. In some preliminary tests with smaller models of different nose shape, high-pressure pulses were generated at cavity collapse in all cases. Further study needs to be done in this area.

*Probe vs. instrumented model*

As mentioned earlier, numerous difficulties encountered with the instrumented-model method of pressure measurement prevented the obtaining of meaningful data for all but a few entries. In figure 14, a pressure signal from one of these isolated entries is compared with a probe signal from a corresponding vertical entry at 110 ft./sec. Reasonably good agreement is observed between both signals.

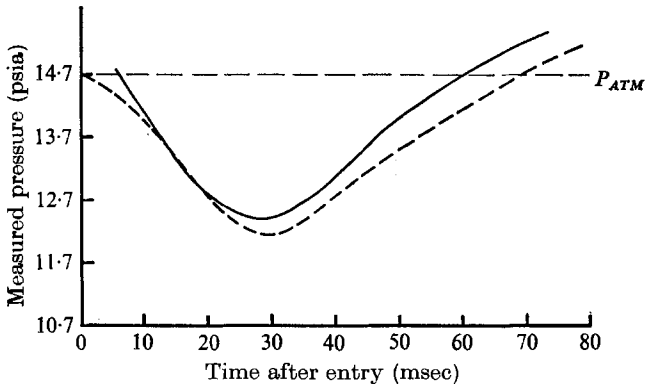


FIGURE 14. Comparison of pressure data obtained by probe and instrumental projectile methods. $U_0$ = 110 ft./sec. —, probe; - - -, instrumented model.

## Summary of results

Results have indicated the pressure drop prior to surface closure is an order of magnitude greater than was previously assumed. As the entry angle (from the horizontal) was decreased, the pressure drop in the cavity also decreased, first very slowly and then more rapidly. For example, cavity pressure for vertical and 60° entries was essentially the same, but was significantly different for 45° entries. The minimum cavity pressure was found to decrease linearly with increasing entry speed over the range velocities tested. As the entry angle was decreased, the minimum entry velocity required to produce a drop in cavity pressure increased. An improved pressure-volume correlation was obtained when true cavity volume rather than outline volume was considered. Cavity pressure during the closed cavity phase, prior to deep closure, was found to behave approximately according to the isentropic relation $p_c V_c^{\gamma} = \text{const}$. The pressure drop and history in the cavity were found to be strongly affected by projectile nose geometry. No appreciable or consistent pressure gradient, either axial or transverse, was found to be present in the cavity. The pressure within the splash sheath was found to be essentially the same as the pressure in the cavity. Near deep closure, a sharp increase in pressure followed by a rapid decay in the form of damped pressure oscillations was noted, indicating that cavity collapse is accompanied by high-pressure pulses.

## REFERENCES

ABELSON, H. 1969 Behaviour of the cavity formed by a projectile entering the water vertically. Ph.D. Thesis, University of Maryland.

BIRKHOFF, G. 1946 Summary technical report of the applied mathematics panel. NDRC **1**, IV, ch. 10.

BIRKHOFF, G. & ISAACS, R. 1951 Transient cavities in air-water entry. NAVORD Rep. 1490, 1951.

HOOVER, W. R. & DAWSON, V. C. D. 1966 Hydrodynamic pressure measurements of the vertical water-entry of a sphere.

MAY, A. 1952 Vertical entry of missiles into water. *J. Appl. Phys.* **23**, 1362–1372.

RICHARDSON, E. G. 1948 The impact of a solid on a liquid surface. *Proc. Phys. Soc. (Lond.)* **61**, 352–367.

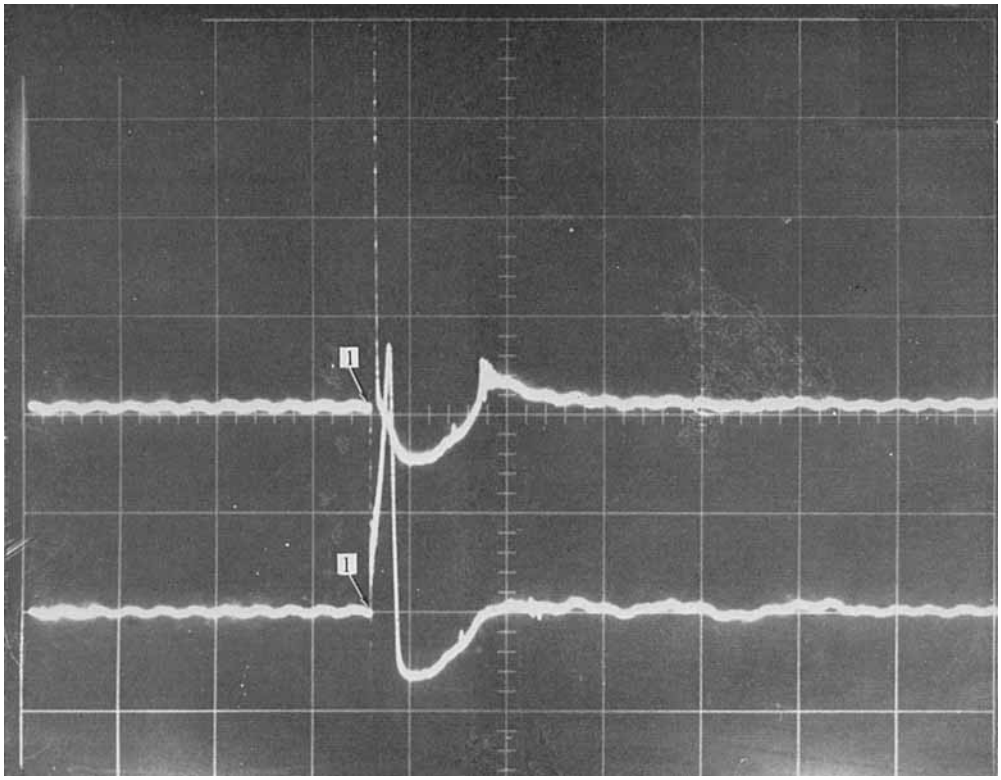

FIGURE 2. Typical pressure data for vertical entry.
6 psi/div.; 50 msec/div.; $U_0$ = 145 ft./sec.

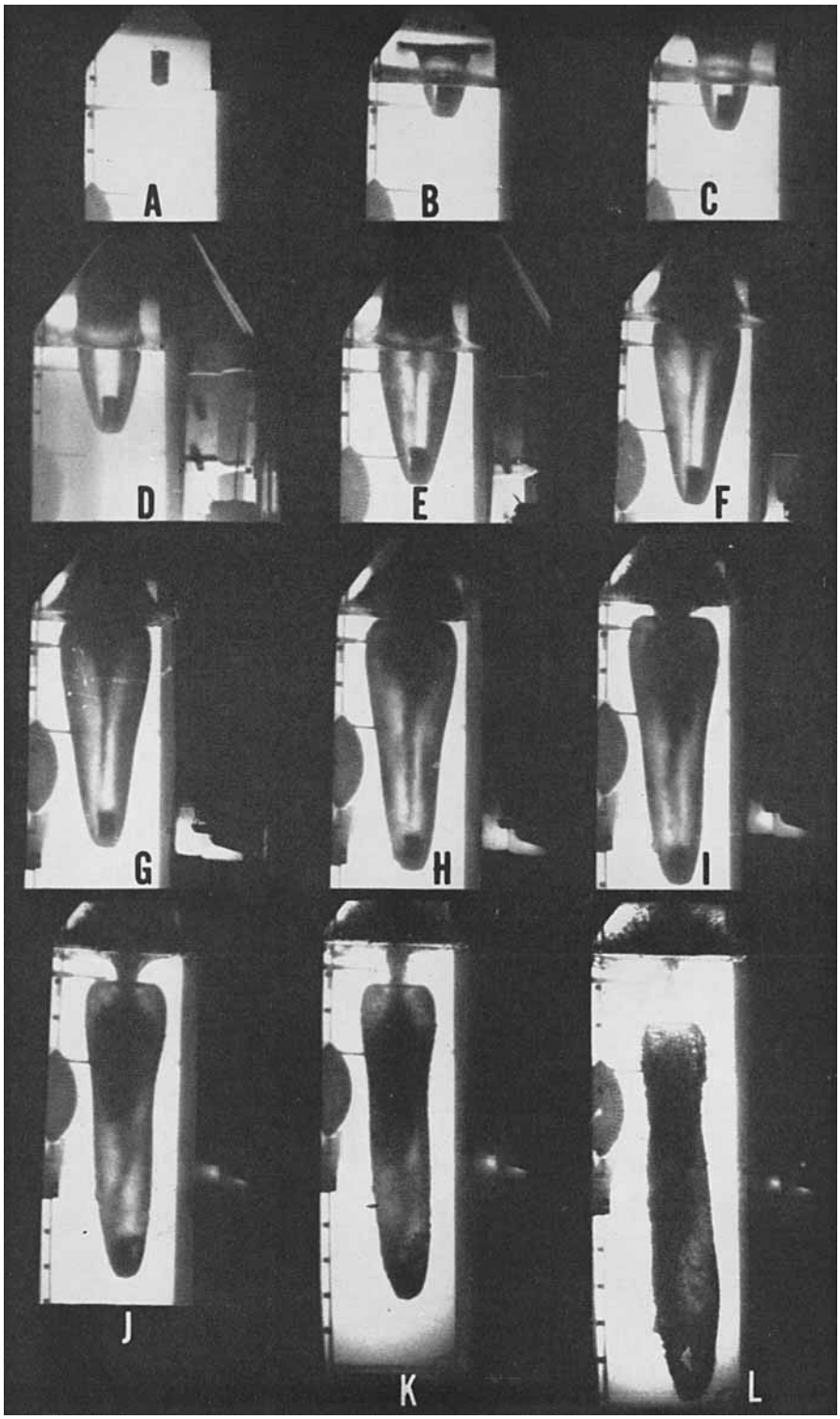


FIGURE 5. Selected cavity photographs corresponding to times denoted in figure 4.

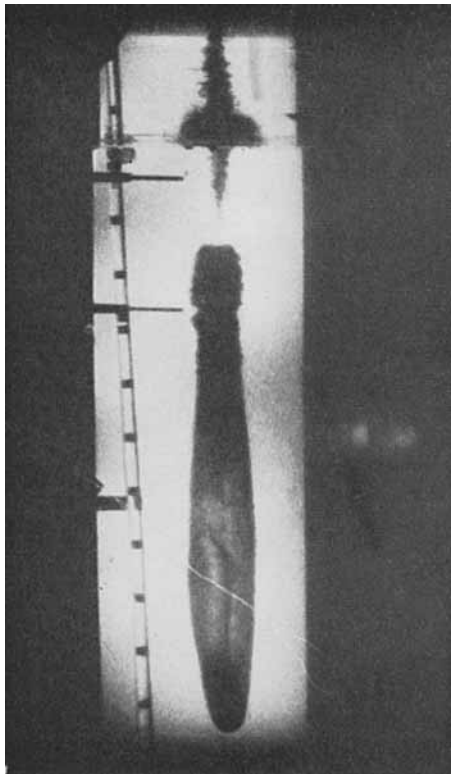

FIGURE 13. Cavity collapse resulting in generation of high-pressure pulses.